Journal of Cardiovascular Magnetic Resonance (2006) **8,** 693–701

ISSN: 1097-6647 print / 1532-429X online
DOI: 10.1080/10976640600723664

informa
healthcare

How to Perform an Accurate Assessment of Cardiac Function in Mice using High-Resolution Magnetic Resonance Imaging

Jürgen E. Schneider, PhD,[1] Frank Wiesmann, MD,[2] Craig A. Lygate, PhD,[1] and Stefan Neubauer, MD[1]

Department of Cardiovascular Medicine, University of Oxford, United Kingdom[1]
Medizinische Klinik, University of Würzburg, Germany[2]

ABSTRACT

High-resolution magnetic resonance cine imaging (cine-MRI) is a method that allows for a non-invasive assessment of left ventricular function and mass. To perform this quantitation, hearts are imaged from the base to the apex by a stack of two-dimensional images. Thus, analysis of myocardial mass and function by cine-MRI does not rely on geometric assumptions. Geometric and functional parameters, such as end-diastolic volume (EDV), end-systolic volume (ESV) or ejection fraction (EF), are obtained by subsequent image segmentation of the respective cine frames in each slice. While this technique has been well established in clinical practice, it is now rapidly becoming the reference method in experimental cardiovascular MRI for accurate quantification of cardiac parameters, thereby aiding the phenotyping of the increasing number of transgenic and surgical mouse models. However, accurate measurement of cardiac functional parameters requires the images to be acquired in short-axis orientation of the heart, which can be difficult to define, particularly in animals with diseased hearts. Furthermore, data analysis can be the source of a systematic error, mainly for myocardial mass measurement. Here, we describe a protocol that allows for a quick and reproducible approach of obtaining the relevant cardiac views for cine-MRI, and we explain how an accurate experimental image analysis can be performed.

INTRODUCTION

Recent developments in transgenic techniques have lead to an enormous increase in genetically modified mouse models of cardiovascular disease. In particular, the ability to specifically knock out, over-express, or mutate certain genes and their products allows one to study the influence of individual genes on cardiac morphology and function in detail. Furthermore, dedicated surgical techniques are becoming more common in laboratories around the world, whereby conditions are generated that closely resemble those found in patients with cardiac disease. For example, coronary artery ligation (CAL) induces myocardial infarction and subsequently heart failure, whereas transverse aortic constriction (TAC) reduces the cross-sectional area of the aorta to cause pressure overload of the heart. This results in progressive hypertrophy of the left ventricle as a compensatory mechanism, eventually leading to heart failure. Most importantly, physiological and pathophysiological conditions of the heart can be investigated in mouse or rat models in much more detail than it would be possible in humans.

In order to investigate the structural and functional effects of gene alteration or the consequences of surgically induced myocardial stress on the hearts of mice, techniques for cardiovascular phenotype characterization are required. The small size of the mouse heart (approximately 1/2000th the mass of a human heart) and high heart rates (∼600 beats per minute [bpm]) impose

Keywords: Magnetic Resonance Imaging, Rodent Models, Cardiac Function, Heart Failure.
Received 11 November 2005; accepted 13 February 2006
This work was funded by the British Heart Foundation.
Correspondence to:
Jürgen E. Schneider
Department of Cardiovascular Medicine
University of Oxford
John Radcliffe Hospital
Headley Way
Oxford OX3 9DU
UK
fax: ++44-1865-287 763
email: jurgen.schneider@cardiov.ox.ac.uk

substantial challenges on phenotyping methods. Echocardiography is frequently used to characterize cardiac function in mice because it is a quick and affordable technique; however, it has a relatively low reproducibility since imaging conventionally is 1D (M-mode) or 2D, and so relies on geometric assumptions for volume calculation. Furthermore, shadowing by the sternum, and limits on spatial resolution prevents accurate analysis of the right ventricle. Magnetic resonance imaging (MRI) is a non-invasive technique that uses intrinsic contrast and is capable of obtaining true 3D information on the heart and the vascular system. This method has so far only been applied in a few centres around the world (e.g., 1–9), but the number of such centers is rapidly expanding, and MRI is bound to become the reference standard for phenotyping the mouse heart.

The focus of this article is to provide a detailed explanation of how to obtain relevant experimental data on global cardiac function in mice and, more specifically, how the cardiac views (i.e., short- and long-axis) can be reproducibly found in normal and diseased hearts. We also show how an accurate data analysis can be performed in order to obtain low inter- and intra-observer variability. Good reproducibility is essential for reliably detecting small changes in cardiac structural and functional parameters using small sample sizes. First, however, we will briefly describe the technical requirements for assessing cardiac function in mice using high-resolution MRI.

MATERIALS AND METHODS

Hardware requirements

The mouse heart's small size requires an optimized hardware set-up: increasing B_0-field strength benefits the signal-to-noise ratio (SNR) and therefore improving spatial resolution and/or reduce experimental times. Specifically cine experiments on mice have been reported on magnetic field strengths between 4.7 T (4) and 11.7 T (6). Dedicated RF-coils such as birdcage coils (2), which are optimized in diameter, length and loading for a particular animal size, should be used to obtain maximal SNR. These coils provide excellent RF-field homogeneity and can also be applied in "quadrature mode," resulting in an additional increase in SNR by up to a factor of $\sim\sqrt{2}$ (10). Furthermore, strong, fast switching gradient systems with high-duty cycle are necessary to apply rapid sequences at high spatial resolution. The gradient coils should be cooled efficiently in order to prevent temperature changes being transferred to the animal, which could result in altered cardiac function.

Animal preparation

Dedicated animal cradles, optimized in diameter and length, are required to maintain stable animal physiology throughout an experiment. Isoflurane anaesthesia (1.0–1.5% in oxygen with a flow rate of 1.5 L/min) is the preferred reagent since the drug is easy to administer and titrate and has the least impact on cardiac function (11). Since the eye closure reflex is suppressed during anaesthesia, ophthalmic lubricating ointment must be applied to the eyes in order to keep them moist. The animal cradle consists of a heating blanket which maintains the core body temperature at 37°C (to be monitored using for example a rectal probe), a nose cone for continuous delivery of the anaesthetic and a scavenging line for anaesthetic gas recovery. Additional lines may be used if cardiac-stimulating drugs such as dobutamine (or MR contrast agents) need to be administered. Cardiac and respiratory signals must be acquired from the animal inside the magnet for monitoring and gating purposes. ECG-information can be obtained with surface-mounted or needle electrodes (~25 gauge) inserted subcutaneously into the forelimbs. The latter is a more robust and sensitive approach in our experience, particularly in diseased animals or mice with ECG distortion. Respiration can be monitored using conductor loops or pressure pads mounted on top of the chest and the abdomen. The mouse is then secured in the cradle using surgical tape, without distorting or compressing the abdominal or chest cavity regions. On recovery after scanning, mice should be provided with a source of heat until they are active and fully recovered from the anaesthesia.

Physiological gating

Physiological gating is required to minimize motional influence of the beating heart and respiration on the MR experiment but also to synchronize the imaging sequence to the cardiac cycle. In general, the degree of motion artifacts in the un-gated MR images is dependent on the number of motion events, the time scale and magnitude of motion within the imaging plane (12) as well as the number of data averages used. In order to obtain virtually artifact-free images, respiratory gating may not be required at 4.7 T (4) but is crucial at 11.7 T (6) as motion artifacts become more pronounced with increasing magnetic field strength (13). Interrupting acquisition during respiration may lead to an intensity modulation in the images, or to additional–non-motion related–artifacts, caused by T_1-modulation of the amplitude and depending on the phase encoding scheme used. These artifacts can be minimized by maintaining steady-state during respiration without data acquisition (6, 14). Devices that are specifically designed to acquire and process mouse ECG's with heart rates between 400–600 bpm and respiratory rates between 20–60 breaths per minute and to interact with the MR scanner accordingly are commercially available. It should also be noted that the ECG acquisition may be prone to MR gradient break-through problems (15), and therefore appropriate suppression measures have to be taken in order to minimize the impact on the sequence timing or to avoid mis-triggering.

Pulse sequence

While refocused steady-state free-precession sequences are frequently used for cardiac MRI on human scanners, they are more difficult to employ at ultra-high magnetic fields due to their sensitivity to susceptibility differences. Thus, in order to assess cardiac function in mice, fast, 2D spoiled gradient echo (GE) type sequences are commonly applied continuously throughout the cardiac cycle as shown schematically in Fig. 1. These sequences saturate spins that are stationary relative to the imaging

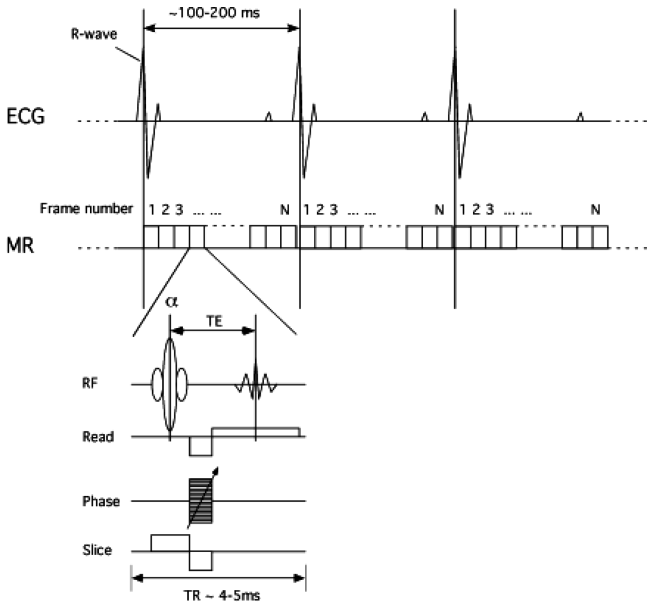

Figure 1. Diagram of a spoiled gradient echo cine sequence used in murine MRI: After the detection of the R-wave in the ECG, the same k-space line is acquired repeatedly with a constant value for the phase encoding gradient. The number of frames N per cardiac cycle depends on the sequence timing and the heart rate of the animal and ranges between 15–30 frames. The illustrated scheme is repeated in the next cardiac cycle with a different value for the phase encoding gradient. Thus, the product of number of phase encoding steps times the number of averages cardiac cycles are required in total to obtain a full cine data set for one slice. If respiratory gating is employed, the scheme is interrupted during respiration (with or without steady-state maintenance) and the imaging time is prolonged.

slice and use the contrast of inflowing (i.e., blood) spins. Thus, myocardial and skeletal muscle appears dark, and blood bright ("bright-blood-contrast") (e.g., 4, 6, 16). The echo times are B_0-field dependent and chosen such that lipid- and water-protons have an opposite phase to enhance the contrast between different tissue types (17). Their values range between 1 to 2 ms. The flip-angle of the sequence needs to be adjusted according to the chosen repetition time and respective relaxation times in order to maximize the contrast between blood and myocardium. Specifically, repetition times of less than 5 ms per frame freeze cardiac motion and are usually kept constant. The number of available frames per RR interval (typically 15–30 frames in mice) is adapted to the respective heart rate. A delay at the end of each cine-train allows for minor variations of the heart rate during the experiment and for residual gradient break-through on the ECG-trace to decay before triggering on the next R-wave. Special care has to be taken to ensure that the relevant frames (i.e., end-diastolic and end-systolic frame) are contained in the acquired cine train (see also section *Problems and Pitfalls*). Finally, the cine-sequence is applied in multi-slice mode, whereby seven to ten contiguous slices (thickness 1 mm) are usually required to cover the entire mouse heart from base to apex.

More recently, murine black-blood cine images have been shown to accurately assess left-ventricular mass and function (18). A double inversion recovery technique was applied at the beginning of a cardiac cycle to suppress the signal from the blood pool and was followed by a cine train in the subsequent RR-interval. While this approach is more time consuming compared to the common bright blood imaging, the black blood preparation improved image appearance for example in myocardial SPAMM tagging, mainly due to the absence of tagged blood in the ventricular cavity (18).

A cine study in a mouse (including the time for setting up the experiment) typically takes approximately 30–45 min, mainly depending on the size of the heart. We routinely scan six animals on a standard scan day.

Overall procedure

The overall procedure of assessing cardiac function comprises the following steps:

1. Preparation of the animal and positioning in the magnet with the heart in the isocenter of the RF-coil.
2. Scouting for the short- and long-axis views.
3. Setting up the MR-scan, including tuning and matching the coil, slab-selective shimming and RF-pulse calibration.
4. Multi-slice, multi-frame MR scans in short-axis orientation.
5. Animal recovery.
6. Off-line data analysis: Manual or semi-automated segmentation of myocardium and ventricular cavity in the end-diastolic and the end-systolic frame for each slice. Calculation of ventricular function.

PLANNING OF THE RELEVANT VIEWS

It is common to display and analyze the heart in a coordinate system, which is defined by the symmetry of the heart rather than by the orientation of the laboratory (i.e., gradient) system. This takes into consideration the elliptical geometry of the heart and minimizes partial volume effects. In the patient/gradient coordinate system, the three orthogonal planes are transverse, sagittal and coronal (Fig. 2A), and in the heart, they are short-axis-, long-axis two- and long-axis four-chamber view (Fig. 2B). These planes are usually double oblique relative to the patient/gradient coordinate system. In the short-axis view, the left ventricle has a characteristic doughnut shape, with the crescent-shaped right ventricle attached to it (Fig. 3A, B). Orthogonal to this view are both long-axis views: the four-chamber view (Fig. 3C, D) and the two-chamber view (Fig. 3E, F). The papillary muscles typically do not appear connected to the ventricular muscle in end-diastolic frames in mid-ventricular slices and can be seen as dark spots inside the bright ventricular cavity (Fig. 3A). However, these views can be difficult to define, particularly in animals with abnormal or diseased hearts. Following the description below allows for a reproducible planning of the views.

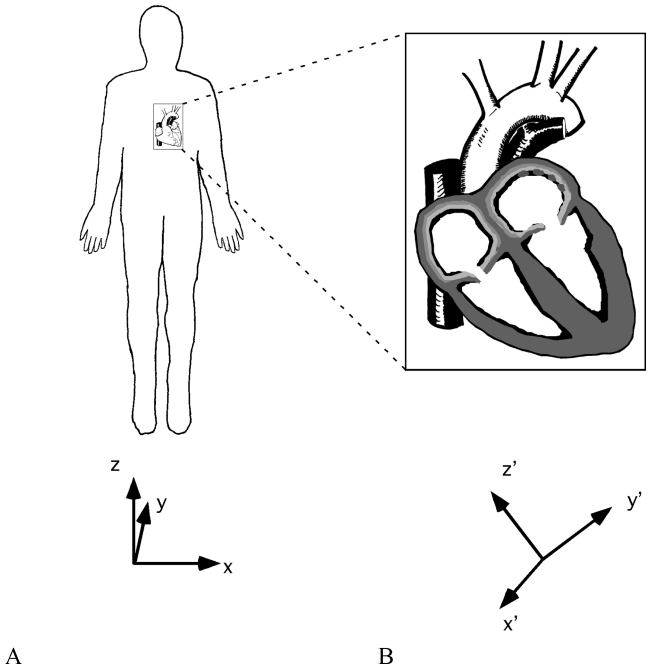

Figure 2. Orientation of cardiac views. (A) Coordinate system (xyz) in laboratory as defined by gradients. The three basic planes are: transverse orientation (xy-plane), which is perpendicular to the long axis of the body, dividing the body into upper and lower sections; sagittal orientation (yz-plane), dividing the body into left and right sections; and coronal orientation (xz-plane), dividing the body into front and back sections, respectively. (B) Reference system as defined by geometry of the heart, which is oblique relative to the coordinate system in (A). The cartoon of the heart shows the long-axis four-chamber orientation (y′z′-plane). The short-axis orientation (x′y′-plane) is perpendicular to the long-axis of the heart. Cutting the left ventricle orthogonal to the short-axis and the long-axis four chamber orientation yields the long-axis two-chamber orientation (x′z′-plane).

Left ventricular short axis view

Once the mouse is positioned in the magnet with the heart in the isocentre, we acquire four axial slices with a gap of 0.5 mm to approximately cover the heart (Fig. 4A–D). This scouting scan is followed by a single-slice scan (labeled s1), which is orientated longitudinally, perpendicular to all axial slices and cuts through the left and right ventricle, as indicated in Fig. 4A–D. We then acquire a second longitudinal slice (s2), which is perpendicular to the first longitudinal image and is orientated through apex and outflow tract of the left ventricle (Fig. 5A). Both long-axis views now allow for planning the short-axis orientation (s3), which is orthogonal to the previous two long-axis views as indicated in Fig. 5A, B. Left ventricular mass and function can eventually be obtained from a stack of multi-frame slices, positioned as scan s3 and covering the heart from base to apex.

Left ventricular long-axis four-chamber views

The left ventricular long-axis four-chamber view (Fig. 3B) shows the atrium and ventricle of the left and the right heart, respectively. It can be obtained by placing the slice orthogonal to scans s2 and s3 as shown in Fig. 5B, C (resulting scan s4).

Left ventricular long-axis two-chamber view

The left ventricular long-axis two-chamber view (Fig. 3C) shows the left atrium and ventricle and is orthogonal to both the short- and the long-axis four-chamber view (i.e., scans s3 and s4).

Planning of image orientation for assessment of right-ventricular function

Assessing right ventricular function requires a slightly modified procedure due to the different geometry of the right ventricle compared to the left ventricle. The exact orientation can be obtained in this case by following the description above up to scan s4. Specifically, the short-axis slices are then positioned orthogonal to the septum rather than the long-axis of the left ventricle (19), as illustrated in Fig. 5D.

Data analysis

All functional parameters characterizing the heart are obtained by manual or semi-automated slice-by slice segmentation of the multi-frame data. In each slice, end-diastolic and endsystolic frames are chosen first, corresponding to the frames with maximal and minimal ventricular volume, respectively. The decision on which frame to segment is aided by viewing the frames in movie mode. The epicardial border is outlined first manually or semiautomatically using a *Lasso-* or *AutoTrace* function. The ventricular volume is subsequently segmented with a threshold tool. While ventricular cavities are easy to segment, left-ventricular mass measurements are much more prone to systematic errors, particularly in the most basal and apical slices due to reduced image contrast or structural complexity of the heart. Thus, special care needs to be taken to only include structures for LV mass in normal hearts that are actively contracting and moving towards the LV cavity centre. The result of a typical image segmentation process is shown in Fig. 6: the white compartment corresponds to myocardial volume and the grey compartment to the ventricular cavity volume. Ventricular mass is obtained by multiplying the myocardial volume with the density of myocardial tissue (1.05 g/cm^3 [20]). Since the heart is fully relaxed in the stack of end-diastolic frames and maximally contracted in the end-systolic one, fewer slices may need to be segmented in the latter case. Moreover, the number of pixels for LV mass in the end-systolic frame are not comparable to the pixel number in the end-diastolic frame of the same slice, but the sum for each frame, i.e., end-diastolic mass and end-systolic mass should agree well with an accuracy of 5% or better. Once the segmentation is completed for all slices and the results are summed, cardiac functional parameters such as stroke volume (SV), ejection fraction (EF) or cardiac output (CO) can be calculated, as summarized in Table 1. It is recommended that each laboratory validates the segmentation process against autopsy first, and also establishes inter- and intra-observer variability.

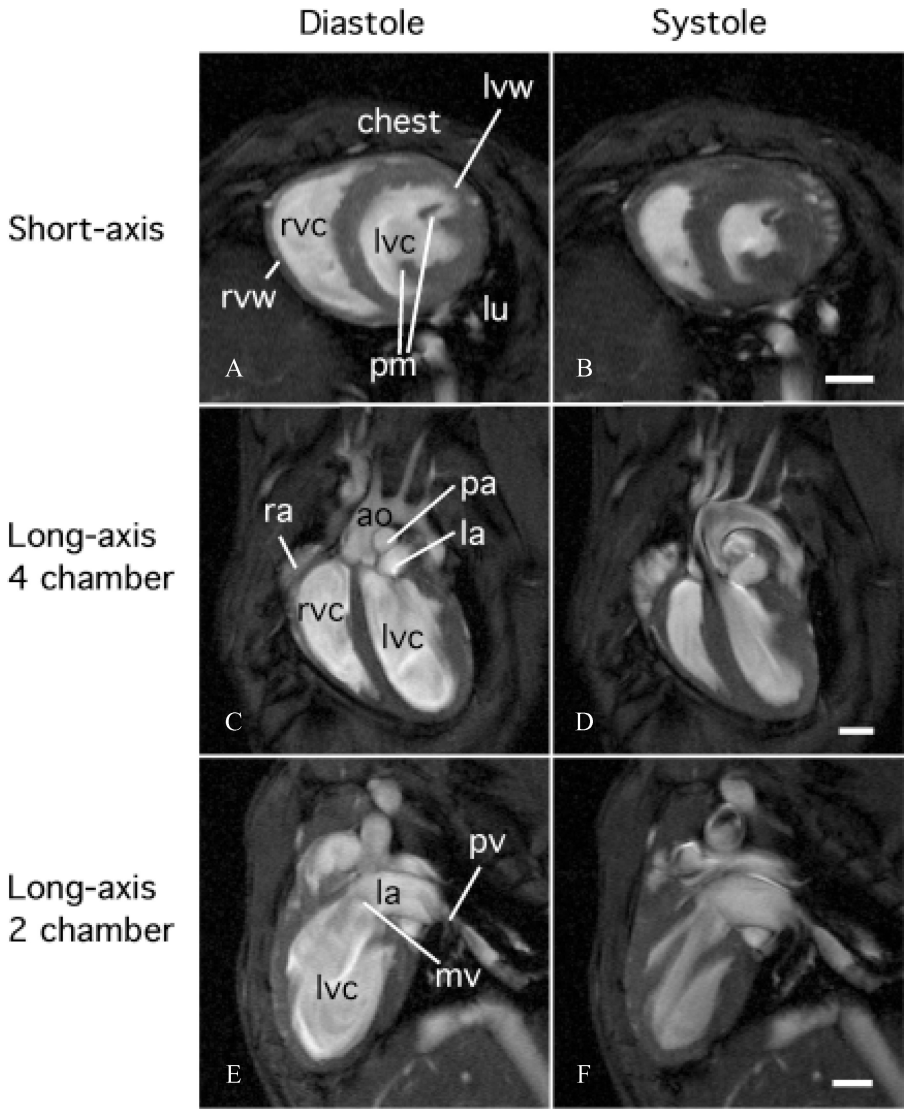

Figure 3. Cine-images of normal mouse heart. Mid-ventricular end-diastolic images through a murine heart in the (A) short-axis orientation, (C) the four-chamber long-axis and (E) the two-chamber long-axis orientation; both long-axis views are orthogonal to the short-axis orientation. Panels (B), (D) and (F) correspond to the respective end-systolic frames. lvc, rvc = left/right ventricular cavity; lvw, rvw = left/right ventricular wall; pm = papillary muscle; lu = lungs; la, ra = left/right atrium; ao = aorta; pa, pv = pulmonary artery/vein; mv = mitral valve. Scale bars: 2 mm.

We found at 11.7 T for left ventricular end-diastolic mass 5 ± 3 and 3 ± 2, for EDV 3 ± 3 and 1 ± 1, and for ESV 6 ± 5 and 3 ± 1 (in %, mean $\pm$ SD, inter- and intra-observer variability) (6).

Measurement of infaret size

Cine imaging can also be used to characterize surgical models of human cardiac disease non-invasively. In chronically failing hearts of rodents (4, 7, 8, 21), the degree of failure (as indicated by the ejection fraction; hearts with an EF <45% may be defined as failing) can be assessed with cine-MRI. Furthermore, in the chronic MI model, hearts can also be stratified according to their infarct size. The infarct is characterized as the area of akinesis. Figure 7 illustrates a typical result of an infarct size measurement in a mid-ventricular slice of an infarcted mouse heart. In the end-diastolic frame, the endo- and epi-cardial circumferences are traced and measured (Fig. 7A) separately from the length of the infarcted tissue. The infarct size can be calculated according to:

$$\text{Infarct size} = \frac{1}{\text{NSLICES}} \sum_{i=1}^{\text{NSLICES}} \frac{1}{2}\left(\frac{I^i_{epi}}{T^i_{epi}} + \frac{I^i_{endo}}{T^i_{endo}}\right) \cdot 100\%. \quad [1]$$

(With T_{Epi}, T_{Endo}—total epi- and endo-cardial circumference of left ventricle; I_{Epi}, I_{Endo}—epi- and endo-cardial length of infarcted tissue, respectively).

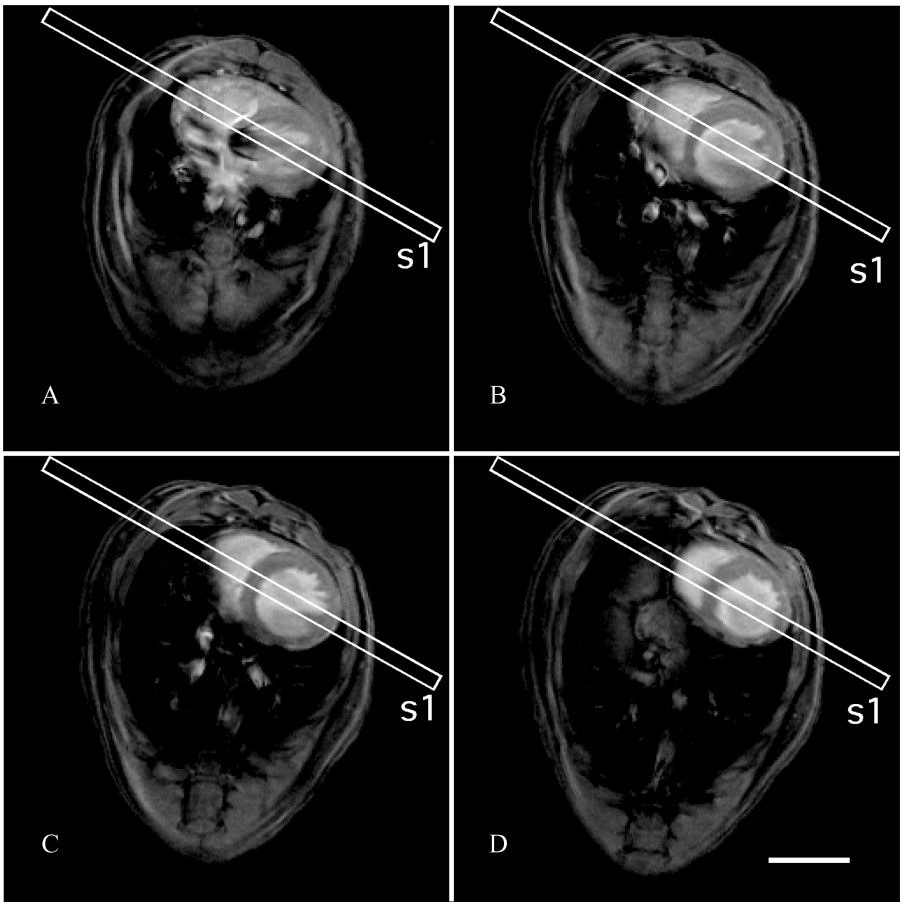

Figure 4. Transverse scout scan. Four transverse slices (thickness 1 mm, gap 0.5 mm) are acquired as the first scout scan, using a segmented gradient echo (GE) sequence. The boxes in (A)–(D) show the orientation of the next longitudinal scout scan (referred to as s1). Scale bar: 2 mm.

In order to distinguish between normal and infarcted tissue when measuring infarct size, the multi-frame capability is crucial, with systolic thickening indicating viable myocardium. Long-term hibernation does not occur in the mouse chronic CAL model, therefore, akinetic areas are considered scar tissue, i.e., non-viable. The infarcted area will also appear significantly thinner, as infarction is almost invariably transmural in the mouse. Measuring infarct size in the mouse is also possible using contrast-enhanced MRI as demonstrated recently (22).

Application

High-resolution magnetic resonance cine imaging (cine-MRI) has been applied successfully to quantify myocardial mass and function in normal (7, 9, 11, 23), chronically infarcted mice (4, 8, 19, 24) and mice with TAC (25). The cine technique also allows the study of developmental changes in cardiac function and mass from neonatal to adult mice (26) or longitudinally in genetically or surgically manipulated mice (16). Applications in transgenic models have, for example, been shown in mice with cardiac hypertrophy (1), in mice with myocardial overexpression of tumor necrosis factor-α (3, 27), and in adult cardiomyocyte-specific VEGF knockout mice (28). The orientation of the magnet bore (horizontal vs. vertical) also merits consideration. We have demonstrated normal cardiac function in healthy and chronically failing mouse hearts positioned vertically in an 11.7 T magnet for approximately one hour (6), but found changes in volumes, ejection fraction and cardiac output in long-term experiments (up to 3 hrs) (21).

PROBLEMS AND PITFALLS

Sequence timing

The R-wave reflects the electrical activation of the ventricles to initiate contraction, and the first frame of the cine sequence corresponds to end-diastole in normal hearts. However, delays, potentially hidden in the gating device and caused by processing or filtering of the raw ECG-signal may generate a time shift between the actual electrophysiologic event in the heart and the (processed) R-wave used for triggering the MR sequence. Thus, this may result in a shift of frames obtained by the cine technique, whereby the first frame no longer represents the end-diastolic frame. In particular, it must be verified that all relevant frames are acquired so that data acquisition throughout the cardiac cycle with a minimum pause for triggering the following R-wave

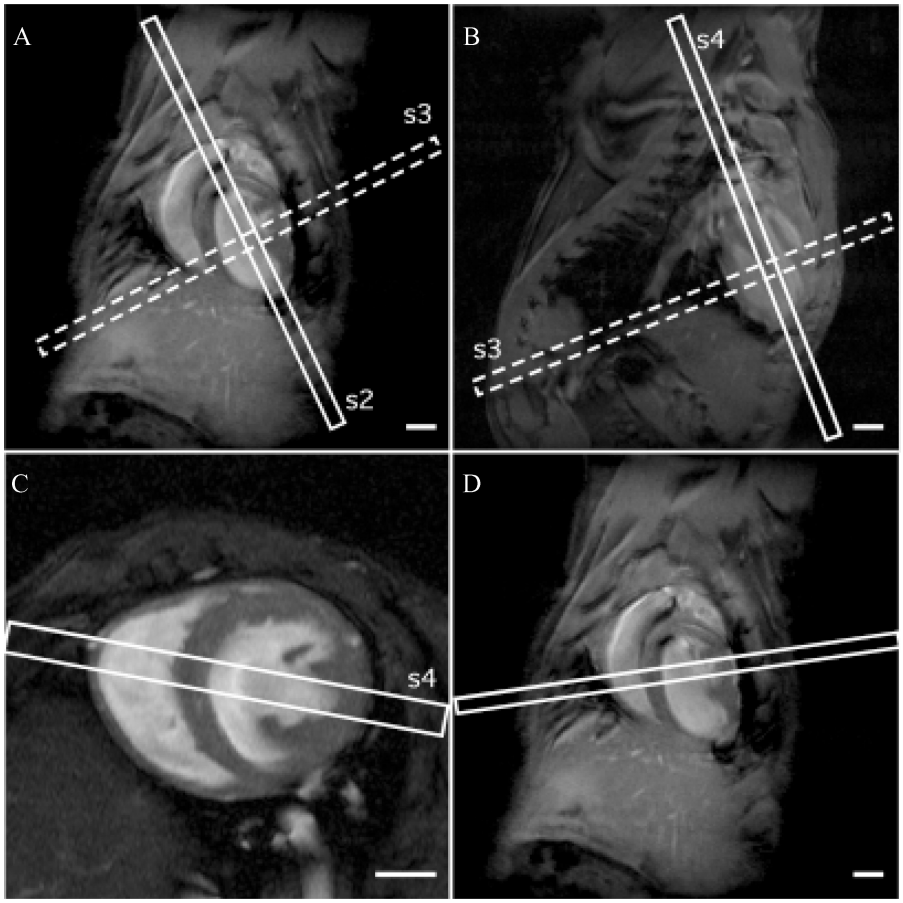

Figure 5. Longitudinal scout scans. (A) Longitudinal scan s1, with the solid white box showing the orientation of the second longitudinal scan s2, cutting orthogonally through the outflow tract and the apex of the levt venricle. (B) Second longitudinal scan s2. (C) Short-axis scan (s3), obtained by placing the slice perpendicular to s1 and s2 respectively (dashed boxes in (A, B). The white box in (B, C) indicates the slice position for obtaining the long-axis four-chamber view (s4). (D) Longitudinal scan s1, with the solid white box showing the orientation of the short-axis slice for assessing right ventricular function. Note, that the slice is orientated orthogonally to the spetum rather than the long-axis of the left ventricle. Scale bars: 2 mm.

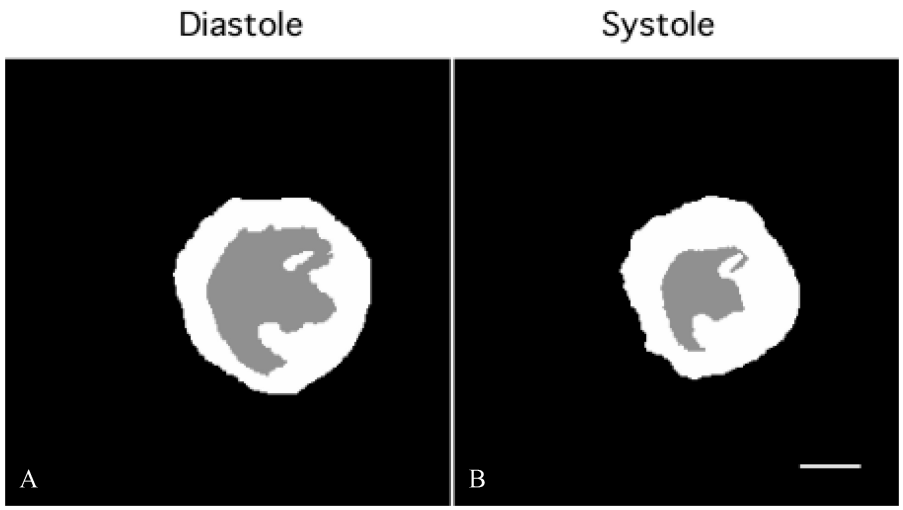

Figure 6. Segmentation of end-diastolic and end-systolic frames shown in Figure 3A, B allows for quantitative measurement of left ventricular mass (white area) and cavity volume (grey area) for each slice and subsequently calculating total cardiac volumes and basic functional parameters. Note that the papillary muscles are counted as ventricular mass and not as part of cavity volume. Scale bar: 2 mm.

Table 1. Relevant cardiac functional parameters

Acronym	Description	Definition	Unit
HR	Heart rate	Beats per minute	bpm
ESV	End-systolic volume		μL
EDV	End-diastolic volume		μL
EDM	End-diastolic left-ventricular volume		mg
ESM	End-systolic left-ventricular volume		mg
SV	Stroke volume	EDV-ESV	μL
EF	Ejection fraction	SV/EDV · 100%	%
CO	Cardiac output	SV · HR	mL · min^{-1}

is guaranteed. Optimal coverage of the entire cardiac cycle is important to avoid missing the end-diastolic and end-systolic frames.

Flow artifacts

A substantially varying heart rate during the acquisition of one slice introduces an additional phase modulation of moving spins (i.e., blood), resulting in an artefact in phase-encoding direction.

Gradient breakthrough

Switching strong gradients may cause mechanical vibrations or may induce a voltage in the loop formed between the electrodes and the animal. This signal may be amplified and superimpose the intrinsic ECG-trace, leading to false triggering. The image contrast and quality can be substantially deteriorated, up to a level where nearly no cardiac contraction can be recognized. Thus, any gradient interference has to be minimized. The gradient breakthrough on the ECG-trace can be reduced by minimizing the area of the loop between the electrodes and the animal during the preparation of the animal prior to the MR scan. Additional measures in the gating device such as filtering or blanking of the gradient noise are the most effective way of eliminating this problem. Finally, additional delays at the end of the multi-frame sequence may be required to allow for any residual gradient noise to decay before the detection of the next R-wave.

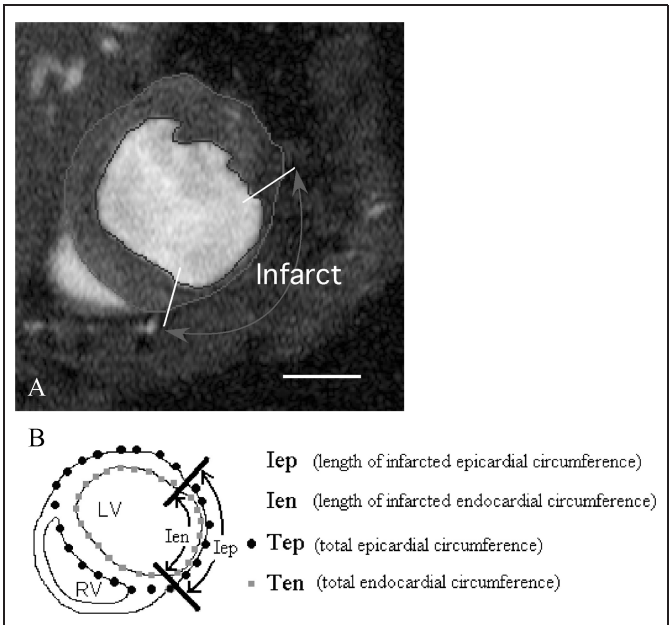

Figure 7. Mid-ventricular end-diastolic frame in the short-axis orientation of an infarcted mouse heart as used for measuring infarct size. (A) Traces of the endo- and epi-cardial circumferences (in dark- and light-grey, respectively). The akinetic area is indicated. (B) Cartoon illustrating the different dimensions required for measuring infarct size.

SUMMARY

In this paper, we describe how cardiac functional parameters of mouse hearts can be obtained accurately and reproducibly. Although described for mice, the procedure in rat models is equivalent. We explain how short- and long-axis views of the heart can be obtained and describe how cardiac parameters such as left ventricular mass and ventricular volumes can be accurately measured. This method should be of major importance for phenotyping the large number of genetically and surgically modified mice and rats.

ACKNOWLEDGEMENTS

We would like to thank our collaborators Prof. Axel Haase (Department of Physics, University of Würzburg, Germany) and Prof. Kieran Clarke (University Laboratory of Physiology, University of Oxford, UK).

The authors (JES, CAL and SN) are also deeply grateful to their co-author, the late Dr. Frank Wiesmann, who played a crucial part in the development of murine cardiac MR.

REFERENCES

1. Franco F, Dubois SK, Peshock RM, Shohet RV. Magnetic resonance imaging accurately estimately LV mass in a transgenic mouse model of cardiac hypertrophy. Am J Physiol 1998;274(2 Pt):H679–83.
2. Hayes CE, Edelstein WA, Schenck JF, Mueller OM, Eash M. An efficient, highly homogeneous radio-frequency coil for whole-body NMR imaging at 1.5 T. J Magn Reson 1985;63:622–8.
3. Kubota T, McTiernan CF, Frye CS, Slawson SE, Lemster BH, Koretsky AP, Demetris AJ, Feldman AM. Dilated cardiomyopathy in transgenic mice with cardiac-specific overexpression of tumor necrosis factor-alpha. Circ Res 1997;81:627–35.
4. Ross AJ, Yang Z, Berr SS, Gilson WD, Petersen WC, Oshinski JN, French BA. Serial MRI evaluation of cardiac structure and function in mice after reperfused myocardial infarction. Magn Reson Med 2002;47:1158–68.
5. Ruff J, Wiesmann F, Hiller KH, Voll Sa, von Kienlin M, Bauer WR, Rommel E, Neubauer S, Hase A. Magnetic resonance microimaging for noninvasive quantification of myocardial function and mass in the mouse. Magn Reson Med 1998;40:43–8.
6. Schneider JE, Cassidy PJ, Lygate C, Tyler DJ, Wiesmann F, Grieve SM, Hulbert K, Clarke K, Neubauer S. Fast, high-resolution in vivo cine magnetic resonance imaging in normal and failing mouse hearts on a vertical 11.7 T system. J Magn Reson Imaging 2003;18:691–701.

7. Wiesmann F, Ruff J, Engelhardt S, Hein L, Dienesch C, Leupold A, Illinger R, Frydrychowicz A, Hiller KH, Rommel E, Haase A, Lohse MJ, Neubauer S. Dobutamine-stress magnetic resonance microimaging in mice: acute changes of cardiac geometry and function in normal and failing murine hearts. Circ Res 2001;88: 563–59.
8. Yang Z, Bove CM, French BA, Epstein FH, Berr SS, DiMaria JM, Gibson JJ, Carey RM, Kramer CM. Angiotensin II type 2 receptor overexpression preserves left ventricular function after myocardial infarction. Circulation 2002;106(1):106–11.
9. Zhou R, Pickup S, Glickson JD, Scott CH, Ferrari VA. Assessment of global and regional myocardial function in the mouse using cine and tagged MRI. Magn Reson Med 2003;49:760–4.
10. Chen CN, Hoult DI, Sank, VJ. Quadrature detection coils—A further 2 improvement in sensitivity. J Magn Reson 1983;54:324–7.
11. Roth DM, Swaney JS, Dalton ND, Gilpin EA, Ross Jr J. Impact of anesthesia on cardiac function during echocardiography in mice. Am J Physiol Heart Circ Physiol 2002;282:H2134–40.
12. Wang Y, Grist TM, Korosec FR, Christy PS, Alley MT, Polzin JA, Mistretta CA. Respirartory blur in 3D coronary MR imaging. Magn Reson Med 1995;33(4):541–8.
13. Wood ML, Henkelman RM. The magnetic field dependence of the breathing artifact. Magn Reson Imaging 1986;4:387–92.
14. Cassidy PJ, Schneider JE, Grieve SM, Lygate C, Neubauer S, Clarke K. Assessment of motion gating strategies for mouse magnetic resonance at high magnetic fields. J Magn Reson Imaging, 2004;19:229–37.
15. Felblinger J, Slotboom J, Kreis R, Jung B, Boesch C. Restoration of electrophysiological signals distorted by inductive effects of magnetic field gradients during MR sequences. Magn Reson Med 1999;41:715–21.
16. Epstein FH, Yang Z, Gilson WD, Berr SS, Kramer CM, French BA. MR tagging early after myocardial infarction in mice demonstrates contractile dysfunstion in adjacent and remote regions. Magn Reson Med 2002;48:399–403.
17. de Kerviler E, Leroy-Willig A, Clement O, Frija J. Fat suppression techniques in MRI: an update. Biomed Pharmacother 1998;52: 69–75.
18. Berr SS, Roy RJ, French BA, Yang Z, Gilson W, Kramer CM, Epstein FH. Black blood gradient echo cine magnetic resonance imaging of the mouse heart. Magn Reson Med 2003;53: 1074–9.
19. Wiesmann F, Frydrychowicz A, Rautenberg J, Illinger R, Rommel E, Haase A, Neubauer S. Analysis of right ventricular function in healthy mice and a murine model of heart failure by in vivo MRI. Am J Physiol Heart Circ Physiol 2002;283:H1065–71.
20. Manning WJ, Wei JY, Katz SE, Litwin SE, Douglas PS. In vivo assessment of LV mass in mice using high-frequency cardiac ultrasound: necropsy validation. Am J Physiol 1994;266:H1672–5.
21. Schneider JE, Hulbert K, Lygate CA, Hove MT, Cassidy PJ, Clarke K, Neubauer S. Long-term stability of cardiac function in normal and chronically failing mouse hearts in a vertical-bore MR system. Magma 2004;17:162–9.
22. French BA. Imaging infract expansion in mice using a contrast-enhanced inversion recovery MRI sequence. J Cardiovasc Magn Reson 2005;7:172–3.
23. Wiesmann F, Ruff J, Haase A. High-resolution MR imaging in mice. MAGMA 1998;6:186–8.
24. Yang Z, French BA, Gilson WD, Ross AJ, Oshinski JN, Berr SS. Cine magnetic resonance imaging of myocardial ischemia and reperfusion in mice. Circulation 2001;103:E84.
25. Lygate CA, Schneider JE, Hulbert K, Ten Hove M, Sebag-Montefiore LM, Cassidy PJ, Clarke K, Neubauer S. Serial high resolution 3D-MRI after aortic banding in mice: band internalization is a source of variability in the hypertrophic response. Basic Res Cardiol 2006;101:8–16.
26. Wiesmann F, Ruff J, Hiller KH, Rommel E, Haase A, Neubauer S. Developmental changes of cardiac function and mass assessed with MRI in neonatal, juvenile, and adult mice. Am J Physiol Heart Circ Physiol 2000;278:H652–7.
27. Franco F, Thomas GD, Giroir B, Bryant D, Bullock MC, Chwialkowski MC, Victor RG, Peshock RM. Magentic resonance imaging and invasive evaluation of development of heart failure in transgenic mice with myocardial expression of tumor necrosis factor-alpha. Circulation 1999;99:448–54.
28. Williams SP, Gerber HP, Giordano FJ, Peale FV, Bernstein LJ, Bunting S, Chien KR, Ferrara N, van Bruggen N. Doubutamine stress cine-MRI of cardiac function in the hearts of adult cardiomyocyte-specific VEGF knockout mice. J Magn Reson Imaging 2001;14:374–82.